UNIVERSITÀ DI PARMA
ARCHIVIO DELLA RICERCA

University of Parma Research Repository

A stand-alone portable potentiostat with parallel channels for smart electrochemical analyses

note finali coverpage

(Article begins on next page)

24 December 2024

AUTHOR QUERIES

AUTHOR PLEASE ANSWER ALL QUERIES

PLEASE NOTE: We cannot accept new source files as corrections for your article. If possible, please annotate the PDF proof we have sent you with your corrections and upload it via the Author Gateway. Alternatively, you may send us your corrections in list format. You may also upload revised graphics via the Author Gateway.

Carefully check the page proofs (and coordinate with all authors); additional changes or updates WILL NOT be accepted after the article is published online/print in its final form. Please check author names and affiliations, funding, as well as the overall article for any errors prior to sending in your author proof corrections.

AQ:1 = Please confirm or add details for any funding or financial support for the research of this article.

AQ:2 = Please specify the degree name for the author Marco Giannetto.

A Stand-Alone Portable Potentiostat With Parallel Channels for Smart Electrochemical Analyses

Andrea Boni, *Member, IEEE*, Valentina Bianchi, *Senior Member, IEEE*, Simone Fortunati,
Marco Giannetto, Maria Careri, and Ilaria De Munari, *Senior Member, IEEE*

Abstract—In recent years portable potentiostats have increased in popularity allowing to perform electrochemical analyses outside the laboratories, moving them to home or point of care (PoC) environments. In this context, the idea of performing multiple acquisitions at the same time is particularly attractive to deal with replicates or with simultaneous multiple quantitative assessments of different analytes, shortening the time required for the analyses and/or increasing data reliability. Multiple parallel channels on a compact and wireless device can maximize the overall system usability. In this article, a multichannel Wi-Fi-based portable potentiostat is described. The device features four independent channels, which can be conditioned with different voltages. The device was designed to minimize the component count and the power consumption, obtaining 23.5 mW per channel. The system was electrically characterized, obtaining an excellent linearity ($R^2 = 0.9999$), a maximum channel-to-channel mismatch of 1% when the maximum current range is selected, and a negligible crosstalk among the channels. Moreover, the multichannel potentiostat was tested in the real case scenario of a semiquantitative evaluation of the anti-tissue transglutaminase target antibodies in celiac disease. Two replicates of IgG and IgA were simultaneously acquired, showing a good capability of separating the positive and the negative samples, with a reduction of the acquisition time of 76% with respect to a single channel solution.

Index Terms—Chemical sensors, electrochemical devices, multichannel, potentiostat, Wi-Fi sensors, wireless sensors.

I. INTRODUCTION

THERE are several contexts in which portable and reliable devices for electrochemical analysis are exploited to provide easy-to-use, rapid, highly selective, and quantitative information on target analytes. Possible areas of application are the detection of biological contaminants in food [1], [2], [3], environmental monitoring [4], [5], [6], and clinical diagnostics [7], [8], [9], [10], [11]. Many of them are based on the use of a potentiostat, i.e., an electronic hardware elaborating the electrical signal generated from an electrochemical reaction.

With reference to this, the main challenge tackled by the researchers is how to implement a compact portable device with cheap components and reduced power consumption without compromising the quality of the tests. It is worth noting that the overall portability of the device strongly depends also on the architecture of the system. In particular, for the development of a completely stand-alone instrument, it is preferable to avoid the use of additional devices for data elaboration and storage. Recently, several portable solutions have been commercialized [12], [13], [14]; however, for their operation, they rely on supplementary devices such as personal computers (PCs) or tablets/smartphones connected via USB and/or Bluetooth. Also, some interesting solutions are available in the literature [4], [15], [16], [17] with some advanced features like the connection to a cloud service, but all require the connection to an external device, limiting the portability and the overall usability.

Moreover, these solutions, as most of the available portable potentiostats, are designed for single analyte detection and are equipped with a single analog front end (AFE) to read and control the electrochemical sensor [4], [15], [16], [17], [18]. Many of these electrochemical acquisitions are time-expensive, with a single experiment easily lasting several minutes. Moreover, replicates are needed to increase the result precision to obtain statistically relevant results. Furthermore, sensor redundancy allows the implementation of advanced fault-tolerant algorithms and data-averaging techniques that can improve system robustness, efficiency, and accuracy [19]. Bioanalytical, pharmaceutical, and clinical applications require simultaneous electrochemical detection that cannot be obtained using a single-channel instrument. For example, parallel measurements of multiple cancer markers are useful for increasing the efficiency of cancer diagnostics and therapy monitoring [20], as well as for considering possible correlations between compounds [9]. Therefore, a potentiostat with multiple acquisition channels would significantly increase the efficiency of the experiments, implementing their parallel execution.

In this article, a multi-channel portable potentiostat with three electrodes for each channel suitable for both quantitative and semiquantitative electrochemical analysis, usable in a large variety of out-of-lab applications, is presented. The device features four completely independent and parallel channels, capable of simultaneously managing, with different voltages, four commercial screen-printed electrodes, each of which

composes a three-electrode electrochemical cell. Thanks to a six-channel analog-to-digital converter (ADC), the current measurement is carried out at the same time for all the channels. The device can be battery-powered and connected, through a Wi-Fi protocol, to a cloud analytics for data storage and elaboration. This allows a simple connection to widespread Wi-Fi networks for sharing data with different users without the need for external devices. Moreover, the cloud service can be interfaced with a web application for the remote control of the device. The aim of this article is the description and the characterization of the hardware device. A detailed description of a possible web application can be found in [18].

The proposed four-channel solution features a scalable architecture that can be easily expanded to meet user needs.

As a case study, an electrochemical immunosensor for the detection of anti-tissue transglutaminase antibodies (anti-tTG) was considered [21]. These antibodies represent reliable biomarkers for the diagnosis of celiac disease, for which both the IgA and IgM isotype of anti-tTG must be quantified. Indeed, it is common for patients affected by celiac disease to display a selective IgA deficiency which, in the absence of IgG quantification, would lead to a false negative outcome of the diagnosis. Therefore, the use of a multi-channel acquisition device is of paramount importance to allow both the simultaneous determination of the IgA and IgG isotypes of anti-tTG antibodies and the acquisition of at least two replicates during a single measurement cycle.

This article is organized as follows. In Section II, the related works are presented; in Section III, the architecture of the system designed is described; in Section IV, the experiments performed to characterize the device are reported and discussed; and in Section V, conclusions are drawn.

II. RELATED WORKS

The key task of a potentiostat device is to measure the current flowing into an electrochemical cell due to a chemical reaction related to the target analyte. The electrochemical sensing systems require two [22] or three electrodes [7]. A three-electrode electrochemical cell includes a working (WE), a reference (RE), and a counter electrode (CE), while in the two-electrode cell, CE and RE are unified. It is worth notingd that, regardless of the number of electrodes in the cell, in order to carry out different types of analyses simultaneously in a multichannel system, it is important to keep independent the electrodes of the different cells under test. In this way, it will be possible to condition the different cells with different voltages according to the analysis to be carried out.

In [23], a multichannel potentiostat is presented. Thanks to four ADCs with single-ended inputs, the device is able to read four independent two-electrode cells simultaneously. The core of the system is a Raspberry PI Computer. Through I2C communication, up to eight potentiostats can be connected. It features a 12-bit DAC for generating the control voltages. Moreover, traditional potentiostats rely on a transimpedance amplifier (TIA) for current measurements. In this case, the authors exploited a shunt resistor, lowering the overall accuracy of the device. The maximum current range is $\pm 1.5\ \mu$A.

It is worth noting that, despite the high number of channels available in this solution considering the eight boards stacked together, the reading of the channels is not simultaneous, but it is serialized through the communication protocol chosen (e.g., I2C). Moreover, notwithstanding the two-electrode system results in a simplified circuitry [22], the three-electrode solution is more advisable since the current deriving from the chemical reaction flows through the CE instead of the reference one, avoiding the change in the potential of the WE [7]. For this reason, the three-electrode solution is the most widely adopted.

In [24] and [25], a compact architecture with 128 channels is reported, where, to reduce the device dimensions, the single potentiostat channel contains only the essential components while the rest of the hardware is time-shared across channels and driven by a single μC. To increase the number of channels, a time division multiplexing technique is exploited. The measurement results are sent to a PC through a UART port, limiting the portability of the device. Moreover, the CE and RE are shared between the parallel channels limiting the possibility of conditioning the electrochemical cells with different voltages. The same limitation applies to the 8-channel potentiostat named "octopoti" presented in [24]. This device cannot be considered a portable solution, as it requires a suitable external data acquisition system to read the outputs. Similarly, in [26], a 16-channel potentiostat requiring a multifunction PC with a data acquisition card to be powered and controlled is presented.

In [27], a six-channel wireless potentiostat is described. In this case, the solution turns out to be quite portable even if the choice of a low-range communication protocol such as Bluetooth does not eliminate the need to have an external device (e.g., PC, tablet, or smartphone) nearby, which acts as a gateway for the acquired data. Moreover, the data elaboration and visualization require the LabVIEW data acquisition system running on an external device.

In [28], a three semi-parallel channels solution is reported. It requires a USB or Bluetooth connection to operate and relies on a smartphone or desktop APP for data processing and visualization. It features a 12-bit DAC and an ADC embedded into the ESP32 Microcontroller. The ADC is in common for the three channels. For this reason, although each of the three channels has dedicated electronics, the data sampling process is performed sequentially, alternating the reading of each ADC pin.

Also, some commercial solutions are available. MultiPalmSens4 and MultiEmStat4 from PalmSens [12] are benchtop instruments with up to 10 and 12 channels, respectively. The portability of these devices is very low, as they communicate over a USB cable and are powered with an external 12V ac/dc adapter or the same USB port. A more portable device is the wireless dual-channel potentiostat Sensit-BT [12]. Another commercial solution is the STAT8000 from Metrohm [15], a portable eight-channel potentiostat. Both are battery-powered and feature a Bluetooth interface. The STAT8000 requires a PC for data elaboration and visualization.
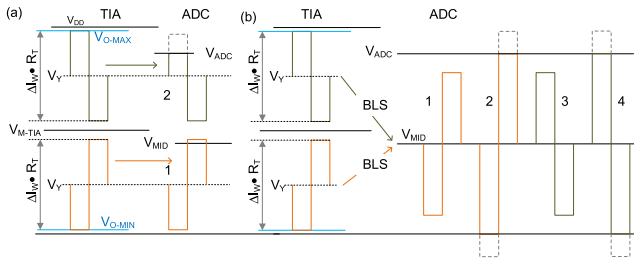
Fig. 1. Schematic of the four-channel potentiostat.

Fig. 2. TIA schematic with feedback network involving the chemical cell. The chemical cell has been modeled with its equivalent electrical circuit (dummy cell).

III. SYSTEM DESIGN

The design of the proposed four-channel potentiostat was optimized for power consumption and component count. To this aim, devices available in the dual or quad configuration were preferred to maintain the same number of components and the same board size of the single-channel implementation [29]. Dedicated ADCs were introduced to improve the quantization error with respect to the A/D conversion channel available in the μC and to implement the simultaneous sampling over the four channels. The analog components were selected for the minimum supply current and with dynamic performance (i.e., bandwidth and conversion speed) compatible with the target configuration (i.e., battery powered) and the frequency of the voltage signal and the output current [29], [30].

The schematic of the potentiostat is shown in Fig. 1. The designed AFE is interfaced with a CC3200 μC [31], a system on a chip (SoC) embedding an IEEE 802.11 compliant Wi-Fi radio [31]. This allows the wireless link capability to be added to the potentiostat device without increasing the component count. Acquired data can be processed on board and then sent to a cloud service for storage and visualization.

For the AFE, the single-ended potentiostat (SEP) architecture, with only two operational amplifiers (opamps) per channel [29], [32], was selected for the cell control and readout, since it exhibits the minimum component count [18], [32]. The former opamp, i.e., A1, is used to control the CE voltage and set the RE voltage, and the latter, i.e., A2, to implement the transconductance amplifier (TIA) for sensing the cell output current. The cell bias voltage, i.e., $V_{\text{bias}} \equiv V_{\text{WE}}$-$V_{\text{RE}}$ (the potentials at the WE and RE pin, respectively), is equal to the difference of the voltage at the positive input pin of A1 and A2, i.e., $V_{\text{bias}} \approx V_Y$-$V_X$, provided that the opamps operate in the linear region. Two quad-DAC AD5696 independently generate for each channel the bias voltage of the TIA, i.e., V_Y, and the voltage signal to be forced at the RE pin, V_X. If the differential pulse voltammetry (DPV) technique is used to assess the concentration of the chemical species, V_X is a pulsed stair-step signal with constant rising and falling steps [29], [30]. The DACs are controlled by the μC through a standard I2C bus.

The AD8608 quad opamp exhibits an input current within tens of picoampere, not to perturb the chemical reaction at the RE pin, and an adequate output current capability to guarantee a short pre-conditioning time of the chemical cell [33].

The TIA opamp A2 is a critical device since it sets the equivalent input noise current of the readout channel. Furthermore, its stability margin is heavily impacted by the RE-WE capacitance (C_{RW}) in the lumped-circuit electrical model of the chemical cell, Fig. 2 [34].

Indeed, this capacitance may be as high as 10 μF, depending on the cell area implementation and the chemical species [35], leading to potential stability issues for the TIA. The schematic circuit for the evaluation of the stability margin and the constraints on the unity-gain bandwidth (GBW) of the involved opamp is shown in Fig. 2.

The equivalent impedance from CE pin to ground (Z_{CE}) usually has a negligible effect on the TIA stability margin, and it is neglected in the following analysis. The feedback network, involving C_T, R_T, and the potentiostat equivalent circuit, introduces a pole and a zero in the loop gain transfer function, $T(f)$. The corresponding frequencies f_{pr} and f_{zr} are approximated by the following equations:

$$f_{pr} \cong \frac{1}{2\pi (C_{\text{RW}} R_H)} \tag{1}$$

$$f_{pz} \cong \frac{1}{2\pi (C_T R_T)} \tag{2}$$

where R_H is the resistance value of the parallel combination of R_{RW} and R_T. In the proposed implementation, the TIA feedback resistance is set within the range from 10 kΩ to 1 MΩ.

The gain programmability is implemented with a pair of four-way solid-state MUXs that allow the selection of one feedback resistance over eight available values [18]. The MUXs are driven by the μC through the general-purpose input–output (GPIO) ports to continuously adapt the TIA gain during the measurement. This background gain calibration aims at maximizing the signal swing at the ADC input, always keeping the TIA opamp in the high-gain region and avoiding the ADC saturation.

The minimum GBW of the TIA opamp is calculated from (1) and (2) to obtain a phase margin higher

Fig. 3. Voltage waveforms at the TIA output and ADC input (zero-mean signal case). (a) Without BLS. Case 1: $V_Y < V_{M-TIA}$; Case 2: $V_Y < V_{M-TIA}$. (b) With BLS between ADC and DAC. Cases 1 and 2: $V_Y < V_{M-TIA}$; cases 3 and 4: $V_Y < V_{M-TIA}$. In cases 1 and 3 the reading range is TIA limited, and in 2 and 4 is ADC limited.

Fig. 4. BLS interfacing the TIA to the ADC.

than 45

$$\text{GBW}_{A2} > \frac{C_{RW} R_H}{2\pi \left(C_T R_T\right)^2}. \tag{3}$$

For the present design, the LTC6082 (quad opamp) was used. It exhibits a typical GBW of 3.5 MHz with a current consumption of 330 μA and can be compensated over the range of feedback resistors.

In the design of the readout channel of the current flowing into the WE terminal (I_W), the signal swing at the TIA output should be carefully considered. Indeed, the reading range of the potentiostat cannot exceed the boundaries set by the output range of opamp A2, at a given value of feedback resistance R_T

$$V_{OMIN} - V_Y \leq I_W \cdot R_T \leq V_{OMAX} - V_Y \tag{4}$$

where V_{OMAX} and V_{OMIN} are the maximum and minimum output voltage of the TIA opamp, corresponding, for the LTC6082, to 3.3 V supply minus 30 and 30 mV, respectively.

A further constraint is introduced by the conversion range of the ADC, assumed from 0 to V_{ADC}

$$0 < V_Y + I_W \cdot R_T \leq V_{ADC}. \tag{5}$$

Restricting the analysis to the case of a zero-mean current signal, the reading range is limited by the lower bound of the TIA-opamp (output) voltage in the case where V_Y is lower than the midpoint of the opamp output range, i.e., $V_{M-TIA} = 0.5 \cdot (V_{OMAX} - V_{OMIN})$, as shown in Fig. 3(a). With V_Y higher than V_{M-TIA}, the reading range is bounded by the ADC conversion range, provided that V_{ADC} is lower than V_{OMAX}.

A further relevant design aspect is the signal-to-quantization-noise ratio (SQNR) of the readout channel. The maximization of the SQNR requires maximizing the signal swing at the ADC input as well. Still assuming a zero-mean $I_W(t)$ signal, the SQNR is estimated by the following formula:

$$\text{SQNR} = 10 \cdot \log \left[\frac{3 \cdot 2^{2 \cdot N_B} \cdot (\alpha_w \cdot \Delta I_W \cdot R_T)^2}{V_{ADC}^2} \right] \tag{6}$$

where N_B is the nominal resolution of the ADC, ΔI_W is the peak-to-peak swing of the cell current, and α_w is equal to one for a square-wave input current or to $1/\sqrt{3}$ for a triangular waveform.

As shown in Fig. 3(b), the mismatch between V_Y, V_{M-TIA}, and the midpoint of the ADC range prohibits achieving the maximum SQNR in (6) with $\Delta I_W \cdot R_T = V_{ADC}$. The problem has been addressed in the proposed design with a dedicated buffer-level shifter (BLS) placed between the TIA and the ADC. As shown in the schematic of Fig. 4, this buffer requires one additional opamp per channel (A3), whereas the opamp A4 is used to buffer a reference voltage (V_{MID}) derived from the supply and shared over all the channels. Furthermore, since the bandwidth of A3 should be compatible with the settling time of the $I_W(t)$ signal, and thus, smaller than the TIA-opamp GBW, the LTC6079 featuring a current consumption of 54 μA was used.
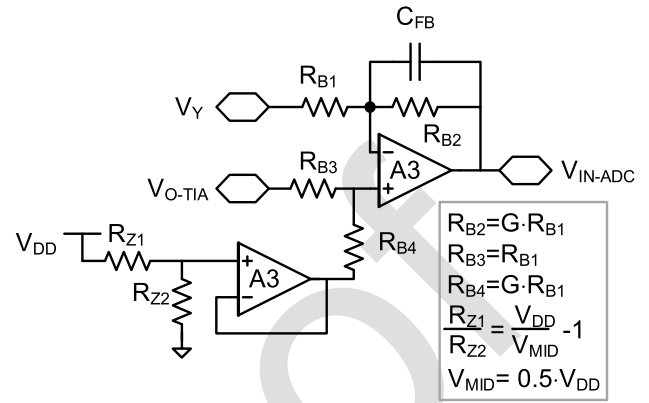
With the resistance settings as in Fig. 4, the buffer output voltage, corresponding to the ADC input signal, is centered at the V_{MID} voltage value and amplified by G

$$V_{IN-ADC} = G \cdot (V_{O-TIA} - V_Y) + V_{MID} = G \cdot I_W \cdot R_T. \tag{7}$$

The reference voltage V_{MID} must be equal to the midpoint of the ADC range, i.e., 1.25 V in our design.

The reading range ΔI_W at the selected TIA gain R_T can be either limited by the TIA or the ADC, depending on the value of G and V_Y. If the ADC saturation occurs before the TIA-opamp saturation, the reading range is ADC-limited, as in cases 2 and 4 in Fig. 3(b). Depending on the setting of V_Y with respect to V_{M-TIA}, the condition for ADC-limited range is

$$V_Y > V_{M-TIA} \rightarrow G \cdot (V_{OMAX} - V_Y) \geq \frac{V_{ADC}}{2} \tag{8}$$

$$V_Y > V_{M-TIA} \rightarrow G \cdot (V_Y - V_{OMIN}) \geq \frac{V_{ADC}}{2}. \tag{9}$$

At the measurement startup, the μC will set the TIA gain at the maximum value. During the measurement, the gain will be decreased as soon as the ADC output approaches the upper or the lower saturation condition, corresponding to conditions (8) and (9), respectively.

If neither condition (8) nor (9) is fulfilled, the reading range is TIA-limited. In this case, the μC will decrease the gain during the measurement at the occurrence of the following condition for the ADC output code D_{O-ADC}:

$$D_{O-ADC} = 2^{N_B-1} + k_O \cdot (2^{N_B} - 1) \cdot \frac{G \cdot \Delta V_O}{V_{ADC}} \tag{10}$$
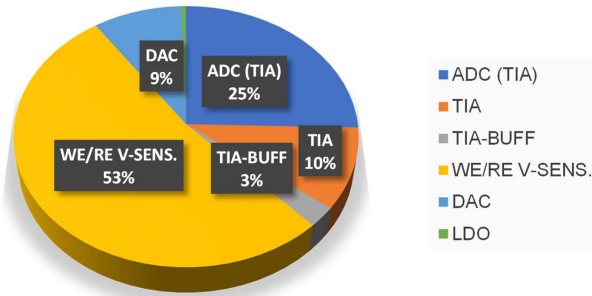
CURRENT CONS. BREAKDOWN

Fig. 5. Current consumption breakdown of the proposed four channels potentiostat. The consumption of the readout circuits for the WE and RE voltage (WE/RE V-SENS) includes the voltage buffer and the related ADC.

TABLE I
CURRENT RANGE, RESOLUTION, AND INPUT NOISE

R_T (kΩ)	$\pm\Delta I_W/2$ (µA)	Resolution (nA)	$I_{IN\text{-}N}$ rms (nA)
10	60	7.6	1.72
100	6.0	0.76	0.173
1000	0.60	0.076	0.017

TABLE II
CHANNEL MISMATCH RESULTS

R_{RW} (Ω)	$\varepsilon_{A,max}$ (mV)	ε_s (%)	ε_i (%)	r^2_{min}
10k	9.2	1	0.5	0.9999
100k	5	0.9	0.4	0.9999
1M	3.1	0.07	0.3	0.9999

where ΔV_O and k_O depends on the position of the V_Y level in the TIA output range, as in cases 1 and 3 in Fig. 3(b)

$$V_Y > V_{M-TIA} \rightarrow \Delta V_O = (V_{OMAX} - V_Y), \quad k_O = +1 \quad (11)$$

$$V_Y \leq V_{M-TIA} \rightarrow \Delta V_O = (V_Y - V_{OMIN}), \quad k_O = -1. \quad (12)$$

In the present design, we used the LTC1408 device integrating six A/D conversion channels. The device was selected for the simultaneous sampling capability, the low power consumption, and the 14-bit nominal resolution, which is suitable for the present potenstiostat [36]. The µC provides the sampling and the clock signals to the ADC through a three-wire serial interface. The same interface allows the acquisition of the output data stream. It is worth noting that the outputs of the four channels have been connected to the same ADC. Hence, the sampling of the outputs of all the channels happens simultaneously. The results are then transmitted to the microcontroller with a serial interface, but this does not affect the timing of the measurements since the transmission is completed between two subsequent measurements.

Additionally, the potentiostat allows the acquisition of the voltages at the WE and RE pins for each cell. These readout channels (not shown in Fig. 1) add a diagnostic capability to the system since the virtual short circuit at the input of A1 and A2 opamp can be continuously monitored during the cell current acquisition cycle. Furthermore, they allow measuring the voltage across WE and RE terminals, which is required in the DPV measurement procedure [29], [30].

The current consumption of the AFE (excluding the µC) is 3.3 mA per channel. A regulated 3.3 V is provided by an onboard low-dropout (LDO) regulator from either the battery or the 5 V USB supply. The consumption breakdown is obtained with circuit simulation (using the SPICE models provided by the manufacturers) and from the current consumption values reported in the component data sheets [36]. The results are shown in the graph in Fig. 5.

With regard to the digital part of the system, a detailed analysis of the power consumption was discussed in [29]. Here, considering the worst case of continuous operation with the µC always active, without low-power mode management between two readings, a current of 3.8 mA per channel should

be considered. Hence, the total current required for both the analog and digital parts is 7.1 mA.

The reading range, the resolution, and the simulated input-current noise (I_{IN-N}), root mean square (rms), for the minimum, i.e., 10 mV/mA, medium, i.e., 100 mV/mA, and maximum, i.e., 1 V/mA, TIA gain are reported in Table I.

IV. RESULTS AND DISCUSSION

A. System Characterization

Several tests were carried out to evaluate the performance of the proposed multichannel portable potentiostat. The single-channel performance was evaluated to assess both the linearity of the response and the output difference among channels with the same voltage signals and load (i.e., channel mismatch). For that purpose, a dummy cell was connected to the input of each channel. A schematic of the dummy cell is reported in the red box in Fig. 2.

Three different values of R_{RW} were taken into account (i.e., 10 kΩ, 100 kΩ, and 1 MΩ). This allows considering different input current ranges (i.e., maximum currents of 62 µA, 6.2 µA, and 620 nA, respectively). The considered ranges are those usually needed in some common applications. For each R_{RW} value, each DAC channel was configured to provide a voltage bias ranging from −0.6 to 0.6 V, and the corresponding V_{out}, i.e., the digital ADC output expressed in volts, was acquired. For each channel combination, an absolute error ε_A was evaluated, corresponding to the difference between the measured V_{out} of two considered channels. In Fig. 6, the measured absolute error between channels is shown, with an R_{RW} value of 1 MΩ.

This analysis was repeated for each possible value of R_{RW}, evaluating the maximum error in the measurement of the output voltage (Table II).

Moreover, a relative error in the slope and the intercept of the fit curve was evaluated as a further parameter of the mismatch between different channels. The relative error in the slope ε_s was defined as

$$\varepsilon_s = \frac{m_{max} - m_{min}}{m_{avg}} \quad (13)$$
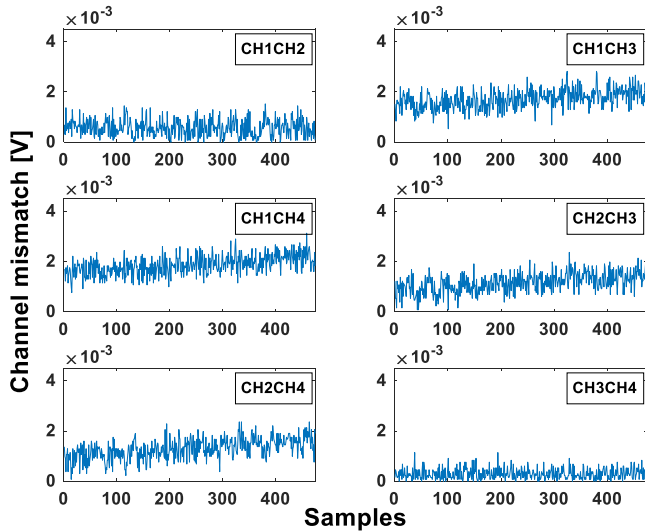
Fig. 6.   Absolute error, corresponding to the difference between the measured V_{out} of the two considered channels, when the 1 MΩ resistor was selected into the dummy cell.

Fig. 7.   Linearity in the four-channel measurements when a 1 MΩ resistor is selected in the dummy cell.

where m_{max} is the maximum value of the fit curve slope, among the four-channel data, given a dummy cell resistance value, m_{min} is the minimum value, and m_{avg} is the averaged value of the four-channel slopes.

Similarly, the relative error in the intercept ε_i was defined as

$$\varepsilon_i = \frac{q_{max} - q_{min}}{q_{avg}} \tag{14}$$

where q_{max} is the maximum value of the fit curve intercept, among the four-channel data, given a dummy cell resistance value, q_{min} is the minimum value, and q_{avg} is the averaged value of the four-channel intercepts. The overall results are reported in Table II.

Finally, the linearity in the V out measurements was evaluated. An example of such an evaluation is reported in Fig. 7, when an R_{RW} value of 1 MΩ is selected.

These reported values show that each channel of the proposed multichannel potentiostat exhibits excellent linearity regardless of the resistance chosen on the dummy cell and then the current sensed by the device. The maximum error due to the channel design difference (e.g., components value and PCB design) is 1%. This is compatible with the tolerance chosen for the gain and feedback resistor.

Once the maximum mismatch among the channels was assessed, tests were carried out to quantify the channel-to-channel crosstalk. As the channels showed negligible mismatch, only channels 1 and 2 were considered for these tests. Two identical dummy cells (Fig. 2) were connected to the channels and configured with a resistance value of 10 kΩ. The onboard DAC was used to generate a sinewave signal with 0.3 V amplitude and 0.5 V offset at different frequencies (i.e., 1, 5, 10, 25, 50, and 100 Hz). This signal was applied to the V_X pin of channel 1 in Fig. 1 and thus replicated to V_{RE} (due to the virtual short circuit at the A1 input). The channel 1 TIA bias voltage V_Y was set to 0.5 V. The V_X and V_Y inputs of
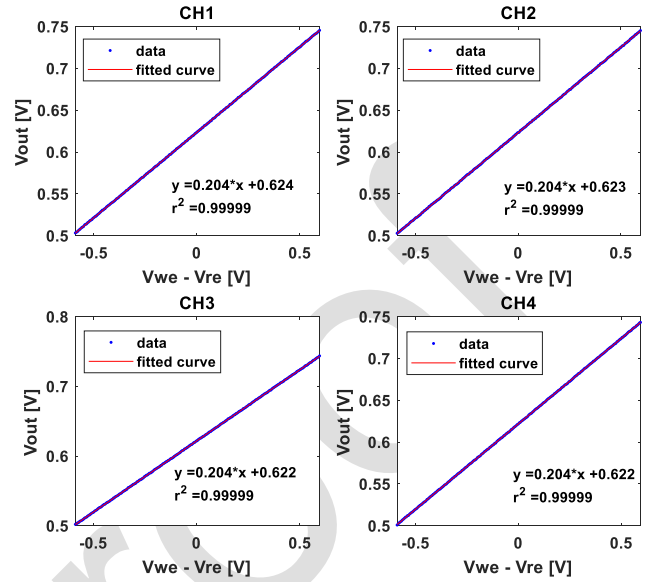
TABLE III
CHANNEL CROSSTALK RESULTS

Input signal frequency (Hz)	FFT amplitude ratio (x1000)
1	2.6
5	4.2
10	5.1
25	4.6
50	4.5
100	2.4

channel 2 were conditioned with the same constant voltage of 0.5 V. The output of each channel was sampled at a frequency of 1 kHz. In Fig. 8, a period of the conditioning signals in the case of a signal frequency of 1 Hz and the corresponding outputs for channels 1 and 2 are shown.

For each frequency considered, the fast Fourier transform (FFT) of both outputs was calculated, and the ratio of the amplitudes at the frequency considered was assessed. In Fig. 9, an example of this evaluation was shown considering a signal frequency of 50 Hz.

The ratio between the FFT amplitudes of the two channels V_{out} at different input signal frequencies is summarized in Table III.

As can be seen from the results, the conditioning signal in a given channel does not influence the behavior of the circuit in another channel, as the ratios in Table III exceed two orders of magnitude for each considered frequency.

B. Case of Study: Simultaneous Detection of IgG and IgA Anti-Tissue Transglutaminase Antibodies

To further demonstrate the behavior of the proposed multichannel potentiostat, the device was tested on the semiquantitative detection of the anti-tTG antibodies directed
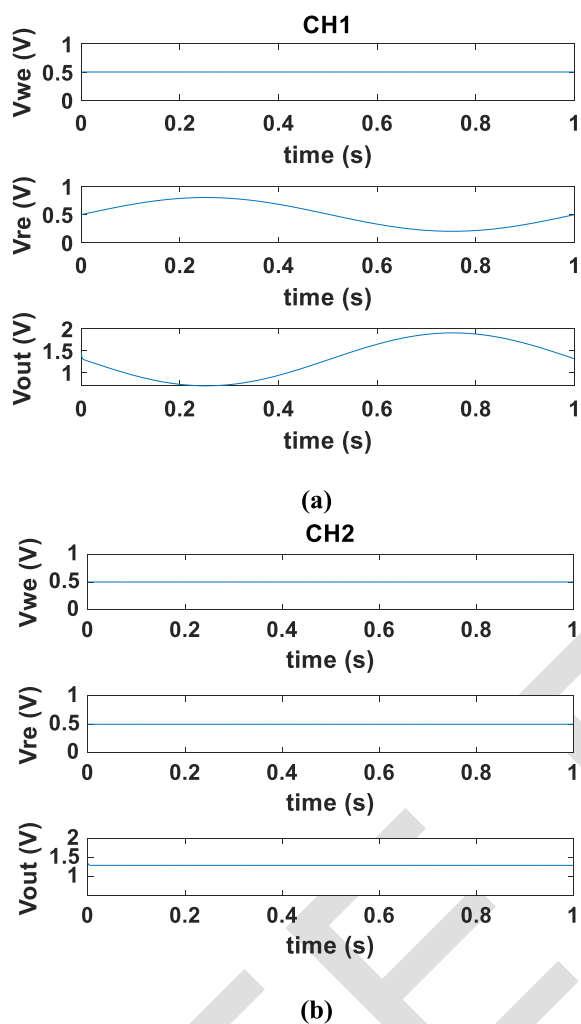
Fig. 8. Input configuration and output measurement in (a) channel 1 and (b) channel 2, for crosstalk evaluation.
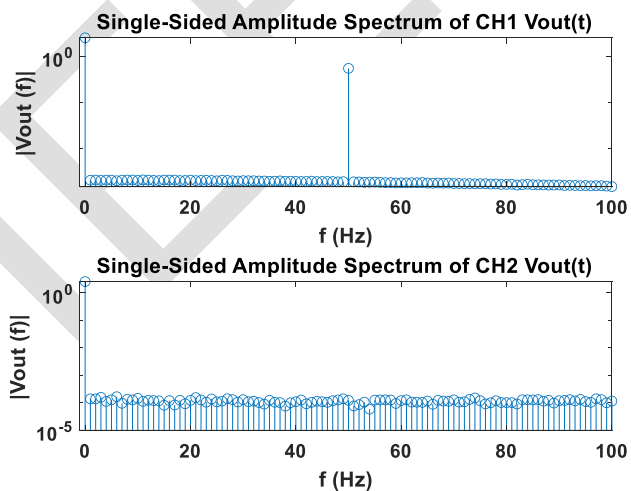

Fig. 9. FFT of the $V_{\text{out}}(t)$ at channels 1 and 2 when a sinusoidal signal with a frequency of 50 Hz is applied to the channel 1.
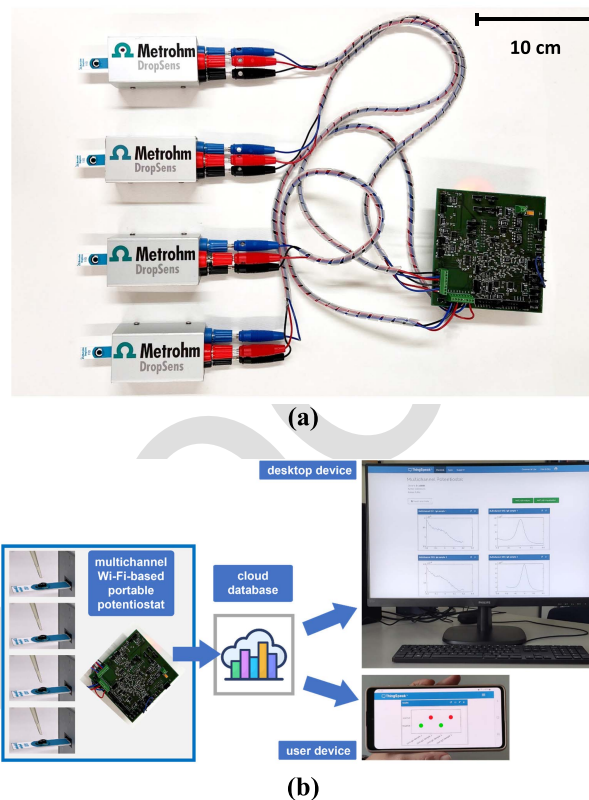

Fig. 10. (a) Prototype of the device designed and used for the tests performed for the semiquantitative analysis of IgG and IgA of the anti-tissue transglutaminase antibodies for celiac disease. (b) Schematic of the operations flow with images of the cloud visualizations.

against the transglutaminase enzyme in its open confor- [481] mation (Open-tTG). To this end, a previously optimized [482] protocol [21] was used for the functionalization of gold [483] nanoparticle-modified screen-printed electrodes (DropSens [484] DRP-110GNP, Metrohm). In particular, the Open-tTG[1] [485] (Zedira) enzyme was chemisorbed on gold nanoparticles, [486] thus allowing the recognition of anti-tTG antibodies by the [487] immobilized enzyme receptor. Detection was achieved using [488] secondary antibodies labeled with alkaline phosphatase, capa- [489] ble of selectively binding to IgG or IgA anti-tTG antibod- [490] ies (Thermo Fisher Scientific). After the addition of the [491] nonelectroactive hydroquinone diphosphate (Metrohm) sub- [492] strate, the enzymatic reaction yields the electroactive hydro- [493] quinone, the oxidation of which generates the signal output. [494] To test the performance of the multichannel device, positive [495] and negative controls of the ZediXclusive Open tTG[1]-Ab [496] (IgA/IgG) ELISA kits were used. These standard solutions [497] have a concentration, respectively, over and below the thresh- [498] old limit of 3 AU/mL for anti-tTG antibodies concentration. [499] These are recognized as specific biomarkers for celiac disease [500] [37]. Both IgA and IgG have to be monitored to avoid possible [501] false negative responses in the case of IgA deficiencies. [502] Considering that at least two replicates are required for each [503] analysis, the use of the proposed four-channel potentiostat [504] allows the entire analysis to be carried out with a single [505] parallel measurement, reducing the overall operation time. [506]

Three replicates of positive and negative controls were [507] tested with the proposed device. In Fig. 10(a), the prototype of [508]

[1]Registered trademark.

the device designed and used for the tests is shown. It is worth noting that, in this prototype version, commercial-off-the-shelf connectors have been used. In a future engineered version, these components can be packed together, reducing the overall dimensions of the device, without affecting its functionalities, as they are only adapters without any circuitry in them.

In Fig. 10(b), a schematic of the operation flow is shown. Once the data have been acquired by the device, they are sent to the cloud service for storage and sharing. The cloud service used is ThingSpeak [38], but other platforms can be exploited as well. Data can be accessed for standard web browsers from PC or mobile devices without the need for dedicated software or APP.

The four electrochemical cells were conditioned with the same parameters: after 3 min when the screen-printed electrodes were left floating to allow for the enzymatic reaction to occur and generate the electroactive hydroquinone, a V_{bias} voltage ranging from -0.2 to 0.2 V was applied. To this aim, V_Y was set at the constant voltage of 1 V, while a variable voltage between 1.2 and 0.8 V was forced at the RE pin through V_X. According to the DPV theory [30], the resulting conditioning voltage should be a staircase waveform with an increasing mean value [30]. It is worth to be noted that the DPV technique has been used in these experiments, but other techniques like chronoamperometry (CA) or cyclic voltammetry (CV) are supported as well. Indeed, CA is based on the application of fixed voltage and measurement of current versus time, and the amplitude of the generated currents is similar to the DPV case [29]. Regarding the CV, the triangular voltage waveform required to bias the cell can be generated by the 16-bit DAC independently for each channel. Furthermore, the reading channel based on the combination of the TIA and the proposed BLS, drives the ADC with a signal always centered at the midpoint of the ADC range. Thus, both positive and negative currents from the WE pin can be properly converted and amplified.

Thanks to the 16-bit DAC, it was possible to set the parameter of the conditioning voltage as those are normally used on benchtop instruments (e.g., AUTOLAB PGSTAT 204 [13]), obtaining 319 measurement points. In particular, the pulse amplitude was set to 50 mV, the step of the pulse low level to 5 mV, the pulse duration to 10 ms, and the time between pulses to 200 ms [30]. A preconditioning time of 30 s, when the cell was kept at -0.2 V, was introduced to preconcentrate the reduced form of hydroquinone, thus increasing the sensitivity of the analysis. To control the time intervals, the μC internal timers were exploited [31]. This ensures a total sample acquisition time, for both IgG and IgA of 4'17" with two replicates against the 17'10" that would occur using only one channel and performing the measurements in sequence. The last case was computed without considering the time needed to change the electrodes at the input of the device.

Differential current waveforms are obtained by subtracting from each other the measured currents at the beginning and at the end of each pulse of the conditioning voltage, as required by the DPV technique. The signals recorded for the three-replicate for both IgG and IgA antibodies are reported in Fig. 11(a) and (b), respectively. Since the peak of
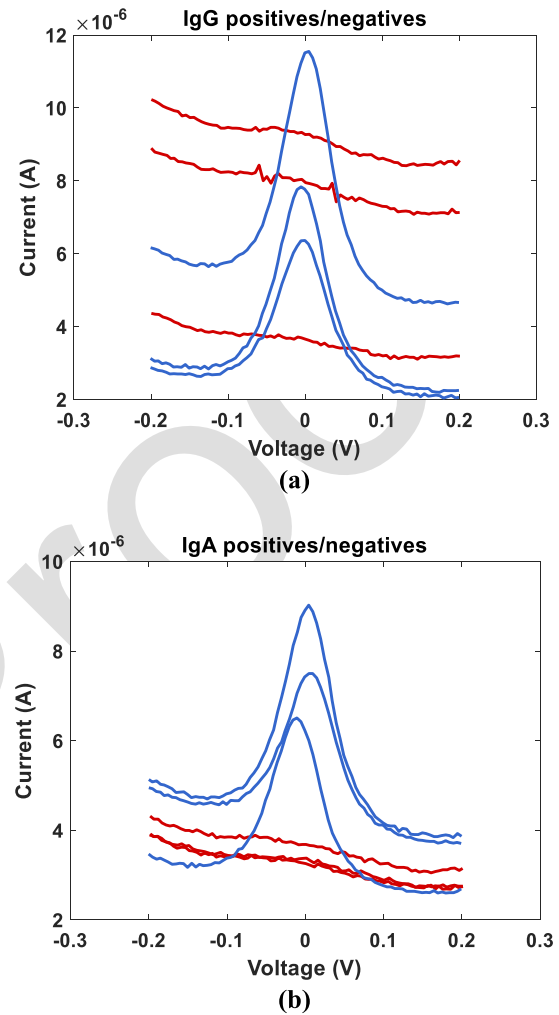

Fig. 11. Positive and negative data acquired for (a) IgG and (b) IgA. Positive samples are drawn with a blue line, and negatives with a red one.

the differential current is related to the concentration of the analyte, it is possible to label a sample as positive or negative through comparison with a predefined threshold.

From the recorded signals, the well-known baseline wandering phenomenon is evident. To overcome this and correctly estimate the current peak, a baseline correction algorithm was performed on the μC platform after the signal acquisition (Fig. 12). The actual baseline was estimated by computing a linear interpolation of the ten first points of the differential current (i.e., blue line in Fig. 12) plus ten relative minimum points. The red line in Fig. 12 represents the baseline, and the blue dots are the point exploited for computing it. The current peak was then computed as the maximum value of the distance between the differential current and the baseline.

As can be observed in Fig. 11, for both IgA and IgG the output signals acquired for the negative controls (i.e., red lines) are negligible, corresponding to current peaks within hundreds of nanoamperes, while intense peaks are recorded for the positive controls (i.e., blue lines).

The boxplot diagrams of the computed current peaks for negatives and positives for IgG and IgA antibodies are reported in Fig. 13(a) and (b), respectively. Again, the clear distinction

Device	Channels	Parallel channels	Max current range (resolution)	Min current range (resolution)	Voltage range (resolution)	Power Consumption per channel	Interface
[23]	32	4 (2 electrodes cell)	±1.5μA	±1.650nA (125pA)	±4V (2mV)	-	Wi-Fi Ethernet
[24], [25]	128	Time multiplexed, 8 independent REs	±3.3μA (100pA)	-	±10V (305μV)	26.7 mW	UART
[27]	6	Shared CE, RE	-	±180nA (5.5pA)	±5V (153μV)	-	Bluetooth
[12]	2	Shared CE, RE	±5mA (300nA)	100nA (6pA)	-2V÷2.3V (537μV)	-	Bluetooth
[13]	8	Shared CE, RE	±80mA (40μA)	±1nA (1pA)	±4V (960μV)	-	Bluetooth
[28]	3	1 (sequential sampling)	±500μA	-	±1.5V (700μV)	-	USB Bluetooth
Proposed	4	4	±62μA (7nA)	620nA (75pA)	±1.65V (50μV)	23.5 mW	Wi-Fi
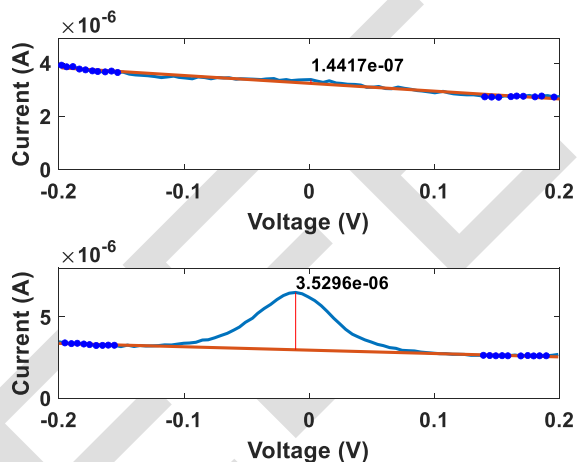
Fig. 12. Baseline correction algorithm with current peak computation for a negative sample (top) and a positive sample (bottom). The red line represents the baseline computed with the linear interpolation of 20 points (marked as blue dots). The actual peak is computed as the maximum value of the distance between the baseline and the differential current (blue line).

between positive and negative controls for both IgA and IgG anti-tTG antibodies is evidenced in the boxplot charts, where a significant difference ($p < 0.001$) was observed.

C. Comparison With Other Works

The comparison of the proposed multichannel potentiostat with other previously described devices is shown in Table IV. As can be seen, the developed device is equipped with four truly independent channels, with simultaneous acquisition and independent conditioning voltages. The Wi-Fi connection, thanks to a longer range than the Bluetooth radio, allows improving portability without the need for an external device nearby, acting as a gateway to the internet. Only a standard Wi-Fi router, which is usually already present in a point of care (PoC) or home environment, is needed to upload data to the cloud. The Wi-Fi link is also exploited in [24]. In that solution, the device was, however, connected to a local PC instead of a cloud service, thus severely limiting the simultaneous sharing of the results with multiple users. It is also worth noting that the system described in [24] is based on a two-electrode cell, waiving the protection of the RE against possible changes in the WE potential [7].

Furthermore, as it can be seen in Table IV, the maximum current range of the proposed device is higher than other devices presented in the literature. The commercial Sensit-BT [12] from PalmSens has a higher maximum current range, but it has only two channels. Also, the commercial solution from Metrohm [13] has some advantages in terms of the number of channels and current ranges, but it requires a PC and proprietary software for data processing and visualization. Finally, the work presented in [28] has a higher current range, but it features a shared ADC for the three channels, so the sampling is sequential and not simultaneous. Moreover, it requires a USB or Bluetooth communication to operate and connect to a desktop or smartphone app for processing and local visualization of the results. Regarding the power consumption, most of the works considered do not report this data. Our solution performs better with respect to [26]. The power consumption of [12] is not reported; battery life is reported instead; however, the battery capacity and a detailed description of the measurement conditions are unknown. They reported a battery life of 12 h at maximum power consumption.
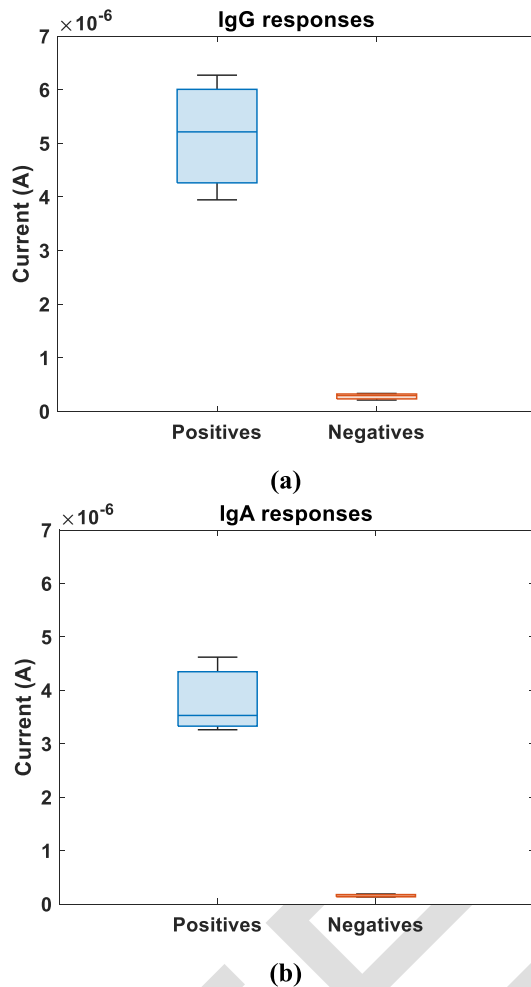
Fig. 13. Boxplot of the current peak of positive samples (blue) and negative samples (red) for the detection of the (a) IgG and (b) IgA antibodies.

For the sake of comparison, we can consider the worst case in which continuous measurements are performed and the microcontroller is always active with no power reduction techniques (e.g., sleep modes management [39]) implemented, and the network processor is idle and connected. Given two 1.5 V, 2700 mAh standard AA batteries, a battery life of 95 h is reached. Moreover, also considering the contribution of the transmission, in the unrealistic case of continuous data transmission, the battery life is reduced to 15 h, which is, in any case, better than the performance reported for the Sensit-BT [12].

V. CONCLUSION

In this article, a multichannel potentiostat for electrochemical analysis with four truly independent channels that can be individually conditioned has been presented. The device is compact and portable, with limited power consumption (23.5 mW), and capable of both onboard processing and communication over a Wi-Fi protocol to eliminate the need for an external device nearby for data processing, viewing, and sharing. The maximum measurable current range is $\pm 62 \ \mu A$, with a resolution of 7 nA. The sensitivity is automatically tuned, defining the current range during the data acquisition through a multiplexer and selecting the best gain of the transimpedance amplifier. The channel-to-channel mismatch has been evaluated, resulting in a maximum relative error in the gain of 1% when the maximum current range is selected. The channel crosstalk has been demonstrated to be negligible. The device shows characteristics that make it usable for different types of electrochemical analysis and then suitable for a large variety of contexts. As a case study, the device was applied for the parallel acquisition of two replicates of IgG and IgA anti-tissue transglutaminase antibodies showing analytical performance fulfilling the diagnostic purposes aimed at evaluating the onset of celiac disease. In this analysis, a reduction of the acquisition time of 76% with respect to the same measurements performed using only a channel is experienced.

In comparison with other commercial devices or published works, the proposed device, while maintaining compatible electrical characteristics, has good portability and low power consumption that makes it suitable for use outside laboratories in home and PoC contexts.

REFERENCES

[1] S. Eyvazi, B. Baradaran, A. Mokhtarzadeh, and M. D. L. Guardia, "Recent advances on development of portable biosensors for monitoring of biological contaminants in foods," *Trends Food Sci. Technol.*, vol. 114, pp. 712–721, Aug. 2021, doi: 10.1016/J.TIFS.2021.06.024.

[2] Y. Lu, Z. Shi, and Q. Liu, "Smartphone-based biosensors for portable food evaluation," *Current Opinion Food Sci.*, vol. 28, pp. 74–81, Aug. 2019, doi: 10.1016/J.COFS.2019.09.003.

[3] R. Umapathi, S. M. Ghoreishian, S. Sonwal, G. M. Rani, and Y. S. Huh, "Portable electrochemical sensing methodologies for on-site detection of pesticide residues in fruits and vegetables," *Coordination Chem. Rev.*, vol. 453, Feb. 2022, Art. no. 214305, doi: 10.1016/J.CCR.2021.214305.

[4] J. Mahato, C. R. Raj, and K. Biswas, "Low-noise potentiostat circuit for electrochemical detection of heavy metals or metalloids," *IEEE Trans. Instrum. Meas.*, vol. 71, pp. 1–9, 2022, doi: 10.1109/TIM.2022.3169560.

[5] Y. Li, J. Tong, C. Bian, H. Dong, J. Sun, and S. Xia, "A portable sensor system for determination of copper ions in waters with Android device," in *Proc. IEEE Sensors*, Oct. 2019, pp. 1–4, doi: 10.1109/SENSORS43011.2019.8956804.

[6] J.-P. Salvador et al., "Portable flow multiplexing device for continuous, in situ biodetection of environmental contaminants," *Sens. Bio-Sens. Res.*, vol. 37, Aug. 2202, Art. no. 100505, doi: 10.1016/J.SBSR.2022.100505.

[7] S. D. Adams et al., "A miniature and low-cost glucose measurement system," *Biocybern. Biomed. Eng.*, vol. 38, no. 4, pp. 841–849, Jan. 2018, doi: 10.1016/J.BBE.2018.07.004.

[8] V. Bianchi, M. Mattarozzi, M. Giannetto, A. Boni, I. De Munari, and M. Careri, "A self-calibrating IoT portable electrochemical immunosensor for serum human epididymis protein 4 as a tumor biomarker for ovarian cancer," *Sensors*, vol. 20, no. 7, p. 2016, Apr. 2020, doi: 10.3390/S20072016.

[9] I. N. Hanitra, F. Criscuolo, N. Pankratova, S. Carrara, and G. D. Micheli, "Multichannel front-end for electrochemical sensing of metabolites, drugs, and electrolytes," *IEEE Sensors J.*, vol. 20, no. 7, pp. 3636–3645, Apr. 2020, doi: 10.1109/JSEN.2019.2959885.

[10] I. Ramfos et al., "A compact hybrid-multiplexed potentiostat for real-time electrochemical biosensing applications," *Biosens. Bioelectron.*, vol. 47, pp. 482–489, Sep. 2013, doi: 10.1016/J.BIOS.2013.03.068.

[11] T. Hongboontry, S. Ponwaranon, S. Sirijongdee, C. Thanachayanont, and P. Pungetmongkol, "Low-cost and portable creatinine electrochemical sensor for non-invasive chronic kidney disease monitoring," in *Proc. IEEE Conf. Nanotechnol.*, Jul. 2021, pp. 159–162, doi: 10.1109/NANO51122.2021.9514318.

[12] *PalmSens-Compact Electrochemical Interfaces*. Accessed: Jul. 25, 2022. [Online]. Available: https://www.palmsens.com/

[13] *Elettrochimica | Metrohm*. Accessed: Jul. 25, 2022. [Online]. Available: https://www.metrohm.com/it_it/prodotti/elettrochimica.html

[14] *CS100 Portable Potentiostat-Corrtest Instruments*. Accessed: Jun. 27, 2022. [Online]. Available: https://www.corrtestinstruments.com/en/extendedseries/1234.html?gclid=CjwKCAjwquWVBhBrEiwAt1Kmwtrz0JcEPvWjuUx-T1-21UlJf_I7mLvPoiF3-d8yCDGIwuZcV3OwpRoCJTgQAvD_BwE

[15] J. Monge, O. Postolache, A. Trandabat, S. Macovei, and R. Burlacu, "Mobile potentiostat IoT compatible," in *Proc. Int. Conf. Sens. Instrum. IoT Era (ISSI)*, Aug. 2019, pp. 1–6, doi: 10.1109/ISSI47111.2019.9043706.

[16] R. Ahmad et al., "KAUStat: A wireless, wearable, open-source potentiostat for electrochemical measurements," in *Proc. IEEE Sensors*, Oct. 2019, pp. 1–4, doi: 10.1109/SENSORS43011.2019.8956815.

[17] S. Sarkar and M. Bhattacharya, "SStat: Wi-Fi and Bluetooth integrated multimodal 'Do-It-Yourself' electrochemical potentiostat," in *Proc. IECON 46th Annu. Conf. IEEE Ind. Electron. Soc.*, Oct. 2020, pp. 5249–5254, doi: 10.1109/IECON43393.2020.9254701.

[18] V. Bianchi et al., "IoT and biosensors: A smart portable potentiostat with advanced cloud-enabled features," *IEEE Access*, vol. 9, pp. 141544–141554, 2021, doi: 10.1109/ACCESS.2021.3120022.

[19] Y. Hu, S. Sharma, J. Weatherwax, A. Cass, and P. Georgiou, "Live demonstration: A portable multi-channel potentiostat for real-time amperometric measurement of multi-electrode sensor arrays," in *Proc. IEEE Int. Symp. Circuits Syst. (ISCAS)*, May 2016, p. 2373, doi: 10.1109/ISCAS.2016.7539064.

[20] J. Wang, "Electrochemical biosensors: Towards point-of-care cancer diagnostics," *Biosens. Bioelectron.*, vol. 21, no. 10, pp. 1887–1892, Apr. 2006, doi: 10.1016/J.BIOS.2005.10.027.

[21] M. Giannetto, V. Bianchi, S. Gentili, S. Fortunati, I. De Munari, and M. Careri, "An integrated IoT-Wi-Fi board for remote data acquisition and sharing from innovative immunosensors. Case of study: Diagnosis of celiac disease," *Sens. Actuators B, Chem.*, vol. 273, pp. 1395–1403, Nov. 2018, doi: 10.1016/J.SNB.2018.07.056.

[22] M. W. Glasscott, M. D. Verber, J. R. Hall, A. D. Pendergast, C. J. McKinney, and J. E. Dick, "SweepStat: A build-it-yourself, two-electrode potentiostat for macroelectrode and ultramicroelectrode studies," *J. Chem. Educ.*, vol. 97, no. 1, pp. 265–270, Jan. 2020, doi: 10.1021/acs.jchemed.9b00893.

[23] P. Pansodtee et al., "The multi-channel potentiostat: Development and evaluation of a scalable mini-potentiostat array for investigating electrochemical reaction mechanisms," *PLoS ONE*, vol. 16, no. 9, Sep. 2021, Art. no. e0257167, doi: 10.1371/JOURNAL.PONE.0257167.

[24] T. R. Molderez, K. Rabaey, and M. Verhelst, "A scalable 128-channel, time-multiplexed potentiostat for parallel electrochemical experiments," *IEEE Trans. Circuits Syst. I, Reg. Papers*, vol. 68, no. 3, pp. 1068–1079, Mar. 2021, doi: 10.1109/TCSI.2020.3048740.

[25] T. R. Molderez, K. Rabaey, and M. Verhelst, "An affordable multichannel potentiostat with 128 individual stimulation and sensing channels," in *Proc. IEEE Int. Instrum. Meas. Technol. Conf. (IMTC)*, May 2020, pp. 1–6, doi: 10.1109/I2MTC43012.2020.9129564.

[26] M. A. Tapsak, J. G. Houseknecht, and P. V. Goode, "A low cost-computer-controlled and powered multichannel potentiostat for general use in development of inexpensive electrochemical sensors," *Instrum. Sci. Technol.*, vol. 35, no. 6, pp. 589–598, Nov. 2007, doi: 10.1080/10739140701651573.

[27] S. Abdullah, M. Serpelloni, and E. Sardini, "Design of multichannel potentiostat for remote and longtime monitoring of glucose concentration during yeast fermentation," *Rev. Sci. Instrum.*, vol. 91, no. 5, May 2020, Art. no. 054104, doi: 10.1063/1.5137789.

[28] I. Anshori et al., "ESPotensio: A low-cost and portable potentiostat with multi-channel and multi-analysis electrochemical measurements," *IEEE Access*, vol. 10, pp. 112578–112593, 2022, doi: 10.1109/ACCESS.2022.3213725.

[29] V. Bianchi, A. Boni, S. Fortunati, M. Giannetto, M. Careri, and I. De Munari, "A Wi-Fi cloud-based portable potentiostat for electrochemical biosensors," *IEEE Trans. Instrum. Meas.*, vol. 69, no. 6, pp. 3232–3240, Jun. 2020, doi: 10.1109/TIM.2019.2928533.

[30] S. C. Rifkin and D. H. Evans, "General equation for voltammetry with step-functional potential changes applied to differential pulse voltammetry," *Anal. Chem.*, vol. 48, no. 11, pp. 1616–1618, Sep. 1976, doi: 10.1021/ac50005a050.

[31] *CC3200 Data Sheet, Product Information and Support | TI.com*. Accessed: Jul. 25, 2022. [Online]. Available: https://www.ti.com/product/CC3200

[32] E. Lauwers, J. Suls, W. Gumbrecht, D. Maes, G. Gielen, and W. Sansen, "A CMOS multiparameter biochemical microsensor with temperature control and signal interfacing," *IEEE J. Solid-State Circuits*, vol. 36, no. 12, pp. 2030–2038, Dec. 2001, doi: 10.1109/4.972154.

[33] *LMP91000 Data Sheet, Product Information and Support | TI.com*. Accessed: Jul. 25, 2022. [Online]. Available: https://www.ti.com/product/LMP91000?utm_source=google&utm_medium=cpc&utm_campaign=asc-sens-null-prodfolderdynamic-cpc-pf-google-eu&_content=prodfolddynamic&ds_k=DYNAMIC+SEARCH+ADS&DCM=yes&_gclid=Cj0KCQjw_viWBhD8ARIsAH1mCd44YdZyBOsSA2r9iu0cjwEm2XxJZ6XmDiByLN94DJ0TEC351OnSzjoaAndYEALw_wcB&=aw.ds#tech-docs

[34] S. M. Martin, F. H. Gebara, T. D. Strong, and R. B. Brown, "A low-voltage, chemical sensor interface for systems-on-chip: The fully-differential potentiostat," in *Proc. IEEE Int. Symp. Circuits Syst.*, vol. 4, 2004, p. 892, doi: 10.1109/ISCAS.2004.1329148.

[35] S. M. Martin, F. H. Gebara, T. D. Strong, and R. B. Brown, "A fully differential potentiostat," *IEEE Sensors J.*, vol. 9, no. 2, pp. 135–142, Feb. 2009, doi: 10.1109/JSEN.2008.2011085.

[36] *LTC1408 Datasheet and Product Info | Analog Devices*. Accessed: Jul. 25, 2022. [Online]. Available: https://www.analog.com/en/products/ltc1408.html

[37] M. Giannetto, M. Mattarozzi, E. Umilta, A. Manfredi, S. Quaglia, and M. Careri, "An amperometric immunosensor for diagnosis of celiac disease based on covalent immobilization of open conformation tissue transglutaminase for determination of anti-tTG antibodies in human serum," *Biosens. Bioelectron.*, vol. 62, pp. 325–330, Dec. 2014, doi: 10.1016/J.BIOS.2014.07.006.

[38] *IoT Analytics-ThingSpeak Internet of Things*. Accessed: Nov. 2, 2022. [Online]. Available: https://thingspeak.com/

[39] A. Boni, V. Bianchi, A. Ricci, and I. De Munari, "NB-IoT and Wi-Fi technologies: An integrated approach to enhance portability of smart sensors," *IEEE Access*, vol. 9, pp. 74589–74599, 2021, doi: 10.1109/ACCESS.2021.3082006.

Andrea Boni (Member IEEE) received the M.Sc. degree in electronic engineering and the Ph.D. degree in information technologies from the University of Parma, Parma, Italy, in 1993 and 1997, respectively.

From 1999 to 2002, he was a Research Assistant with the Department of Information Engineering, University of Parma. Since 2002, he has been an Associate Professor of electronics with the University of Parma, where he is the responsible for the Analog IC Design group. He has authored more than 90 scientific papers and two U.S. patents. He was a Co-Founder of Silis S.r.l., Parma, a university spin-off company involved in the design of high-performance analog and mixed-signal integrated circuits. His research interests include memory accelerators with analog in-memory computing, A/D converters, integrated sensor nodes, and sensor interface circuits.

Dr. Boni has been the Technical Committee of the IEEE Custom Integrated Circuits Conference. He is actually an Associate Editor of the IEEE TRANSACTIONS ON AGRIFOOD ELECTRONICS and a Member of the Editorial Board of *MDPI Electronics*.

Valentina Bianchi (Senior Member, IEEE) received the B.Sc. and M.Sc. degrees in electronic engineering and the Ph.D. degree from the Department of Information Engineering, University of Parma, Parma, Italy, in 2003, 2006, and 2010, respectively.

She is currently a Research Associate with the University of Parma. She has participated in several national and international projects. She has authored or co-authored over 50 papers in international journals or proceedings of conferences. Her current research interests include the design and validation of sensors for human activity recognition, sensors for electrochemical applications, and digital systems implemented on FPGAs, with a special focus on the design of hardware for machine learning algorithms and arithmetic circuits.

Dr. Bianchi is an Associate Editor of the IEEE TRANSACTIONS ON INSTRUMENTATION AND MEASUREMENT.

Simone Fortunati was born in 1990. He received the M.Sc. degree in biomolecular chemistry and the Ph.D. degree in chemistry from the University of Parma, Parma, Italy, in 2016 and 2020, respectively,

He is currently working as Fixed-Term Research Assistant with the Department of Chemistry, Life Sciences and Environmental Sustainability, University of Parma, within the "PON Ricerca e Innovazione" program of the Italian Ministero dell'Università e della Ricerca. His current research interests include employment of innovative bioreceptors for the development of biosensors, aimed at the detection of viral infections and point-of-care testing, voltammetric genoassay for revelation of genetic material involved in tumor-related pathologies, and immunosensors for assessment of antibody response generated through vaccination. He has authored and coauthored 12 articles in the above areas.

Marco Giannetto was born in Messina, Italy, in 1973. He received the degree in chemistry and the Ph.D. degree from Parma University, Parma, Italy, in 1996 and 2000, respectively.

He is currently an Associate Professor of analytical chemistry with Parma University, where he teaches analytical chemistry and "sensors and screening techniques" for the bachelor's and master's degrees in chemistry. He is currently the Co-ordinator of the Interdivisional Group "Sensors" of the Italian Chemical Society, having been elected for the three-year period 2022–2025. His current research interests include the design, realization, characterization, and validation of new chemical sensors and biosensors based on different transduction mechanisms with applications in clinical diagnosis and point-of-care, food safety/quality control, and environmental monitoring. He has authored or coauthored 63 articles in the above areas.

Maria Careri has been a Full Professor of analytical chemistry with the Department of Chemistry, Life Sciences and Environmental Sustainability, University of Parma, Parma, Italy, since 2001 and she was the Head of the Department of Chemistry from 2011 to 2016. She was the President of the Division of Analytical Chemistry, Italian Society of Chemistry, from 2007 to 2009. She was the Director of the National School "Analytical and Bioanalytical Methods Based on Mass Spectrometry" organized by the Division of Analytical Chemistry and the Division of Mass Spectrometry, Italian Society of Chemistry from 2005 to 2014. She was the Scientific Director of the International Course "METROFOOD-RI: Traceability and Comparability of Results in Food Measurements" organized in 2021 by the School of Advances Studies on Food and Nutrition, University of Parma, within the H2020 METROFOOD-RI Preparatory Phase project. She is the Principal Investigator of the national PNRR project on "METROFOOD-IT——Strengthening of the Italian Research Infrastructure for Metrology and Open Access Data in support to the Agrifood" and of an European project on metrology, "European Partnership on Metrology Call 2021——Green Deal (EURAMET)." Her primary research interests encompass the development and application of hyphenated methods in separation sciences, and the development of novel materials for miniaturized extraction techniques and ambient mass spectrometry techniques. She has also been working for several years on the development of innovative immunosensing devices in the field of food safety and clinical diagnostics.

Prof. Careri has been a member of the International Advisory Board of Analytical and Bioanalytical Chemistry (Springer) since 2008.

Ilaria De Munari (Senior Member, IEEE) received the M.Sc. degree in electronic engineering and the Ph.D. degree in information technologies from the University of Parma, Parma, Italy, in 1991 and 1995, respectively.

In 1997, she joined the Department of Information Engineering (presently the Department of Engineering and Architecture), University of Parma, as a Research Assistant and since 2004 has been an Associate Professor of electronics. She has authored or coauthored more than 100 papers in technical journals or proceedings of international conferences. Her past research interests include the reliability of electronic devices and the design of electronic systems for active assisted living. In this framework, she was involved in several European projects. Her current research interests include the design of digital systems based on microcontrollers and FPGA. In particular, she is dealing with the design of sensors for human activity recognition, electrochemical applications, and for the evaluation of the battery state of charge through machine learning algorithms.

Dr. De Munari is an Associate Editor for the journal IEEE ACCESS.